

See discussions, stats, and author profiles for this publication at: <https://www.researchgate.net/publication/26877670>

# Thermoreversible Gelation of Poly(vinylidene fluoride-co-hexafluoro propylene) in Phthalates

ARTICLE *in* THE JOURNAL OF PHYSICAL CHEMISTRY B · OCTOBER 2009

Impact Factor: 3.3 · DOI: 10.1021/jp907047b · Source: PubMed

---

CITATIONS

3

READS

40

## 5 AUTHORS, INCLUDING:



[Dr. P. Jaya Prakash Yadav](#)

Advanced Centre of Research in High Ener...

9 PUBLICATIONS 85 CITATIONS

[SEE PROFILE](#)



[Vinod K Aswal](#)

Bhabha Atomic Research Centre

392 PUBLICATIONS 4,901 CITATIONS

[SEE PROFILE](#)



[Pralay Maiti](#)

Indian Institute of Technology (Banaras Hi...

102 PUBLICATIONS 3,632 CITATIONS

[SEE PROFILE](#)

## Thermoreversible Gelation of Poly(vinylidene fluoride-co-hexafluoro propylene) in Phthalates

P. Jaya Prakash Yadav,<sup>†</sup> Vinod K. Aswal,<sup>‡</sup> P. U. Sastry,<sup>‡</sup> A. K. Patra,<sup>‡</sup> and Pralay Maiti<sup>\*</sup>,<sup>†</sup>

School of Materials Science and Technology, Institute of Technology, Banaras Hindu University, Varanasi 221 005, India,  
Solid State Physics Division, Bhabha Atomic Research Centre, Trombay, Mumbai 400 085, India

Received: July 24, 2009; Revised Manuscript Received: September 10, 2009

The thermoreversible gelation of poly(vinylidene fluoride-co-hexafluoro propylene) copolymer have been studied in a series of phthalates,  $\text{Ph}-(\text{COO C}_n\text{H}_{2n+1})_2$  with  $n = 1-8$ . The gelation rate increases with increasing aliphatic chain length up to  $n = 6$ , and the gelation phenomena does not occur for higher  $n > 6$ . The fibrillar morphology is evident for dried gels whose dimension (both lateral and thickness) becomes shorter and thinner with increasing  $n$ . The structures of the gels formed in various phthalates have been investigated by small-angle neutron scattering and small-angle X-ray scattering techniques, suggesting sheet-like structure, where the interplaner distance increases with increasing aliphatic chain length. The scattering intensity  $I(q)$  decreases with  $q$  according to the Ornstein-Zernike model, where  $q = (4\pi/\lambda) \sin \theta / (2\theta)$  ( $2\theta$  and  $\lambda$  are scattering angle and wavelength of neutron) and the correlation length,  $\xi$ , assigned to the average distance between the neighboring crystallites, also increases with increasing aliphatic chain length of diesters. The detailed thermal analyses and phase diagrams of the copolymer gels have been studied in a wide range of phthalates. Further, polymer-solvent complexes leading to the formation of two distinct compounds have been reported. A systematic change of compound composition has also been observed in the whole range of phthalates studied here. On the basis of electronic structure calculation, a model has been proposed to elucidate the conformation of copolymer chain in presence of various phthalates and their complexes, which offer the cause of higher gelation rate for longer aliphatic chain length up to  $n = 6$ , no gelation phenomena occurs for  $n > 6$ , and formation of two copolymer-solvent compounds. The mechanical properties (storage modulus and viscosity) decrease with increasing aliphatic chain length of phthalates and realignment of fibrils occurs at particular frequency depending on the strength of fibrillar gels.

### Introduction

The sol to gel transformation of a polymer solution can provide various interesting features such as response of the semisolid materials against electric field, pH, stress, and solvent absorptive power. The gelation occurs through the formation of networks by cross-linking of polymer chains in the solvent, either physically or chemically.<sup>1–7</sup> Thermoreversibility of the polymer gels added an extra flavor in physical gels as compared to chemical gels. Sufficiently strong secondary/primary forces are operative in the junction points that combine different parts of the polymer in gel phase. Cho et al.<sup>8</sup> first reported thermoreversible gelation of poly(vinylidene fluoride) (PVDF) in  $\gamma$ -butyrolactone. Since then, several groups have studied physical gelation of fluoropolymers in various solvents as the differences in interaction between polymer and solvent may lead to different kind of gelation behavior and mechanism.<sup>9–15</sup> Recently, we have reported the gelation behavior of PVDF in a series of phthalates.<sup>16</sup> The fibrillar morphology of dried gels, crystallites as the cross-linking points of the gels and a sheet-like structure of dried gels, have been presented. The fibrillar network structures were produced due to polymer-solvent interactions and the fibrils became thinner with increasing the length of aliphatic chain ( $n$ ) in phthalates. The correlation length

and interplaner distance of the gels depend on the aliphatic chain length of diester (phthalates). Unfortunately, the gelation behavior of any fluoro-copolymer has not been studied in the literature.

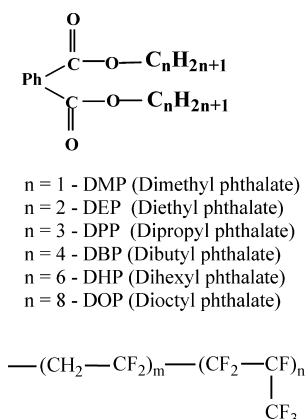
Poly(vinylidene fluoride-co-hexafluoro propylene) is a technologically important copolymer having piezo- and pyroelectric properties because of its availability in different crystalline forms. The potential use of the copolymer gels is in polymer battery, membrane, and other soft materials. The structure of cross-link points, morphology, and the formation of molecular compounds of these gels are usually complicated and are driven by the interactions between solvent molecules and polymer chains having two different monomeric units. Phthalate is an aromatic diester containing  $>\text{C}=\text{O}$  group and can exist in both cis- and trans- form with very little difference in energy (less than 1 kcal/mol). The carbonyl group may interact with dipoles present in polymer molecules, and thereby, it can form molecular complexes. The phase diagram and complexation have been studied for homofluoropolymer and other polymers.<sup>12,14,17–21</sup> The complex formation in copolymer has not been studied yet and might be interesting as there are two different monomers with enough dipole moment available in same molecule for compound formation. Further, the gelation of polymers occurs either via liquid-liquid phase separation or spinodal decomposition followed by the crystallization. The crystallite formation has been the main reason for gelation in fluoropolymers and small-angle neutron scattering (SANS) has been extensively used for size and distribution of the crystallites for other polymers.<sup>22–26</sup>

\* To whom correspondence should be addressed. E-mail: pmaiti.mst@bhu.ac.in.

<sup>†</sup> School of Materials Science and Technology, Institute of Technology, Banaras Hindu University.

<sup>‡</sup> Solid State Physics Division, Bhabha Atomic Research Centre.

**SCHEME 1: Chemical Structure of Phthalates with Varying Aliphatic Chain Length ( $n$ ) and the Structure of HFP Copolymer Used in This Work**



Because of neutron's shorter wavelength, local concentration fluctuation in gels can be worked out in terms of correlation length. The scattering pattern would be governed by the size and distribution of the crystallites as the crystallite–crystallite correlation is stronger than any other correlations. SANS studies of homofluoropolymer indicated the layered structure of microgel clusters both in gels and dries gels.

In this work, we have studied the thermoreversible gelation of poly(vinylidene fluoride-co-hexafluoro propylene) in phthalates with different aliphatic chain length to examine the influence of aliphatic chain length of diesters on gelation kinetics, morphology, structure, and thermal properties. To have the detailed molecular patterns in gel fibrils, small-angle neutron scattering and small-angle X-ray scattering have been conducted on gels to reveal the size and the distribution of the crystallites. The results of SANS and SAXS are phenomenologically analyzed with different models. The attempt to construct the temperature–concentration phase diagram and related thermodynamics may shed light onto the nature of molecular complexes formed between the solvents and the copolymer. Finally, a plausible mechanism has been given to elucidate all the gelation behavior, its kinetics, cessation of gelation, and the formation of two distinct compounds through molecular modeling (electronic structure calculation). The dynamic mechanical properties of gels in various phthalates have also been measured.

## Experimental Section

**Materials and Methods.** A commercial poly(vinylidene fluoride-co-hexafluoro propylene), henceforth, termed HFP copolymer (SOLEF 11008), Ausimont, Italy, of melt flow index 24 g/10 min at 230 °C under 5 kg load, was used in this work ( $M_w = 6.6 \times 10^5$ , PDI = 3.1 measured by using GPC). Phthalates were obtained either from Loba Chieme, or from Merck, and were used as received. The chemical formula of different phthalates has been presented in Scheme 1, mentioning varying aliphatic chain length ( $n$ ). For the preparation of gel, a predetermined amount of polymer was dissolved in weighed amount of solvent (phthalate) at 200 °C to make a homogeneous solution, and then it was quickly transferred to a fixed temperature liquid bath and allowed until the solution completely freezes. Gelation behavior in each phthalate is reported as a function of polymer concentration and temperature. To prepare dried gel, HFP–phthalate gels were immersed in cyclohexane in a Petri dish at room temperature to replace phthalates gradually by low boiling cyclohexane. Cyclohexane was

replaced by a fresh set to achieve the replacement equilibrium at a faster rate in every 12 h.<sup>13</sup> This process was repeated for 10 days for complete removal of phthalate from gel. After decanting cyclohexane, resulting gels were initially dried at room temperature, followed by under reduced pressure at ambient temperature for 3 days to keep the morphology intact. To observe the effect of guest solvent, we dried the gels only under heat treatment as well without using any guest solvent like cyclohexane for comparison purpose.

**Gelation Kinetics.** Homogeneous HFP solutions were made in different phthalates in the concentration range of 2–20% (w/v) in test tubes, and then it was quickly transferred to a predetermined fixed temperature liquid bath and watched until the solution completely freezes upon tilting. Here, it is to be noted that the gelation time (>90 s) is sufficiently higher than quenching time (around 60 s). The corresponding time where no flow of the sample was observed by tilting the test tube was considered as the gelation time,<sup>3,7,13</sup> and the inverse of gelation time ( $t_{\text{gel}}^{-1}$ ) was taken as the gelation rate at that particular concentration and temperature. The gelation rates in all phthalates were measured in the similar fashion.

**Morphological Investigation.** The morphology of the gels was investigated by using scanning electron microscope (SEM) and transmission electron microscope (TEM). The surface morphology of the dried gels was examined with a LEO 435 VP instrument operated at 15 kV. All the samples were gold-coated by means of a sputtering apparatus before observation. Both the thickness and lateral dimension of the fibrils were measured from several micrographs (30 distinct fibrils), and the populations of fibril dimensions (both lateral and thickness) have been constructed. Thereafter, the distribution of fibril diameter and lateral dimension has also been constructed for two phthalates. The TEM study was done by making fine powder of 10% (w/v) dried gel and fishing them onto a carbon coated grid followed by drying at 50 °C under vacuum for one day. The morphology of the dried gel was observed in a TEM (Technai G<sup>2</sup>) operated at 100 kV.

**Small-Angle Neutron Scattering (SANS).** SANS experiments were performed on the spectrometer at the Dhruva reactor at Bhabha Atomic Research Centre, Mumbai, India.<sup>27</sup> The data were collected in the scattering vector ( $q$ ) range of  $0.17 \text{ nm}^{-1} \leq q \leq 3.5 \text{ nm}^{-1}$ . The scattering from the samples, 10 wt % polymer in respective phthalates, were corrected for the solvent and background contributions, the incoherent scattering which originates due to hydrogen atoms in the sample. The lower  $q$  range was fitted separately with Ornstein–Zernike and other models. The characteristics length ( $\Lambda_c$ ) was calculated using the equation  $\Lambda_c = 2\pi/q_m$ , where  $q_m$  is the scattering vector  $q$  corresponding to the peak position of the shoulder in the scattering pattern. The temperature was kept constant at 30 °C during every measurement.

**Small-Angle X-ray Scattering (SAXS).** SAXS measurements were done on dried gels prepared using the small angle goniometer mounted on the 12 kW Rigaku rotating anode X-ray generator with Cu K $\alpha$  radiation. The intensities were measured by transmission method using a scintillation counter system with pulse height analyzer. Scattered intensities  $I(q)$  from each of the four samples were recorded in steps of the scattering angle  $2\theta$ . The measured intensities were corrected for absorption and slit smearing affects.<sup>28</sup>

**Differential Scanning Calorimetry (DSC).** The gel melting temperature and heats of fusion of gels at different solvents were measured in a Mettler 832 DSC instrument. The samples (small quantity) were heated at the scan rate of 10 °C/min. The peak

temperatures and the enthalpies of fusion were measured from the endotherms using a computer attached with the instrument. After the first melting, the gels were cooled down at a constant rate of 10 °C/min to find the gelation temperature, and the heats of gelation were measured in a similar manner. Further, a second heating was taken to ensure the amount of crystallinity/heat of gelation and gel melting temperature after the formation of gel in a controlled cooling environment. The DSC was calibrated with indium before use.

**Molecular Modeling.** To comprehend the polymer chain conformation and extent of interaction in gels in presence of solvents, molecular modeling has been carried out through energy minimization program to understand intermolecular interactions involved between HFP and phthalates with various aliphatic chain lengths. We have initially optimized α-HFP, experimentally observed conformation, and also phthalate molecules independently. A semiempirical AM1 method, as concerned in Chem3D Ultra 7.0, was used to obtain the optimized geometries. Those optimized structures were then used to understand the dipole–dipole interactions, believed to be the governing factor for gel formation between the >C=O groups of phthalate and >CF<sub>2</sub> and >CF<sub>2</sub>CF(CF<sub>3</sub>) groups of HFP. We have modeled HFP as a truncated chain consisting of minimum 12 monomer units (considering alternating vinylidene fluoride and hexafluoro propylene unit).

**Dynamic Mechanical Characterization.** Frequency dependence of oscillatory shear moduli in the liquid state were measured, using dynamic frequency sweep tests, on Rheologica (model: Nova) using parallel plate geometry (25 mm) at 40 °C keeping the strain amplitude of 0.05 to maintain linear response of the sample. The measured angular frequency  $\omega$  for oscillatory shear experiment was kept in the range from 0.2 to 800 rad/s. The storage moduli, loss moduli, and complex viscosities were measured as a function of angular frequency for 10 wt % gels in different phthalates.

## Results and Discussion

**Kinetics of Gelation.** The gelation rate of HFP in various phthalates has been measured as a function of concentration and temperature. Figure 1a shows the gelation rates ( $t_{\text{gel}}^{-1}$ ), measured by using test tube tilting method, at different concentrations,  $c$ , of HFP in DMP, DEP, and DBP at 40 °C. The gelation rate decreases with decreasing HFP concentration but it increases with the aliphatic chain length of phthalate, e.g., DMP ( $n = 1$ ) to DBP ( $n = 4$ ). This trend was observed up to  $n = 6$  (DHP), and it does not form gel in dioctyl phthalate ( $n = 8$ ). This indicates a solvent dependency phenomenon, where the basic nature of the solvents is the same (diester).<sup>16</sup> When the experimental points of gelation are extrapolated to  $t_{\text{gel}}^{-1}$  tends to zero, the value corresponding to concentration axis would provide the measure of critical gelation concentration ( $C_g^*$ ), below which gelation phenomena cannot occur at that particular temperature. The  $C_g^*$ s of HFP are 6.5, 5.9, and 5.3 wt % for DMP, DEP, and DBP, respectively, showing the aliphatic chain length dependency on gelation rate. The  $C_g^*$  is a function of temperature and is of interest because of the concentration at which the molecular clusters begin to overlap in dilute solution, which is a necessary precondition for gelation to take place. Figure 1b shows the gelation rate of HFP in phthalates at different temperatures, keeping the concentration same (10 wt %). Clearly, the gelation rates decrease at higher temperatures due to the delayed formation of microgel clusters as a consequence of greater mobility. Further, the relative rates of gelation in various phthalates remain same. For a particular

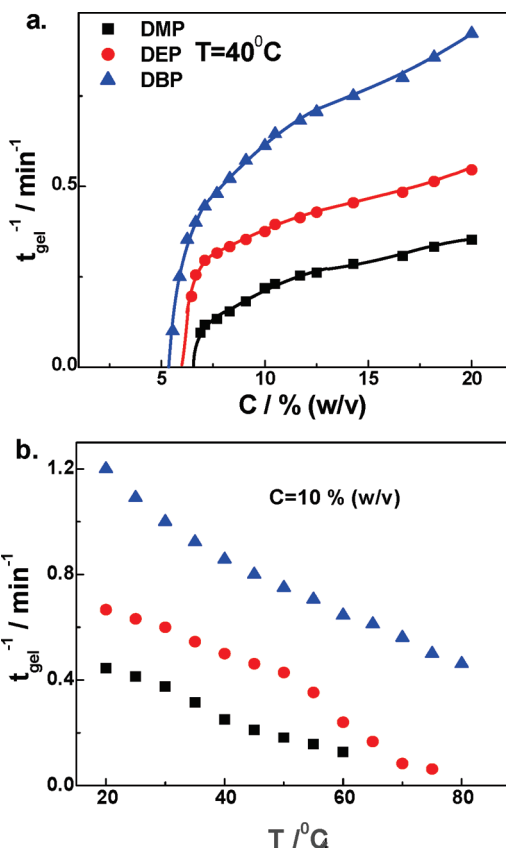


**Figure 1.** Gelation rate vs (a) concentration at 40 °C and (b) temperature for 10% (w/v) of HFP in (solid black square) DMP, (solid red circle) DEP, and (solid blue triangle) DBP. The solid line in (a) are the guide to eye, and the extrapolated curves indicate the critical gelation concentration,  $C_g^*$ .

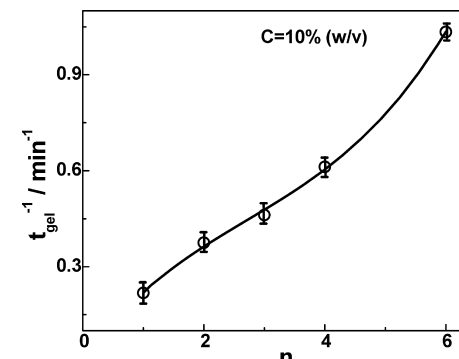


**Figure 2.** Gelation rate as a function of aliphatic chain length ( $n$ ) in phthalates for polymer concentration 10% (w/v) and at 40 °C.

concentration, the gelation rate increases with aliphatic chain length (Figure 2) and is valid for both concentration and temperature dependent experiments. In contrast, the gelation of HFP does not occur in dioctyl phthalate ( $n = 8$ ), indicating a limitation of complex formation up to a certain aliphatic chain length ( $n = 6$ ) beyond which polymer–solvent complexation cannot take place, the same phenomena we observed for pure PVDF gelation.<sup>16</sup>

**Morphology.** Surface morphologies of dried gels in phthalates have been presented in Figure 3a. The morphologies of the dried gels are of fibrillar type with decreasing fibril length and width upon increasing aliphatic chain length of diesters. The three-dimensional fibrillar networks are evident for all the solvents, but the cluster size is small for lower  $n$  (e.g., DMP) and is quite large in higher aliphatic chain length (DBP)

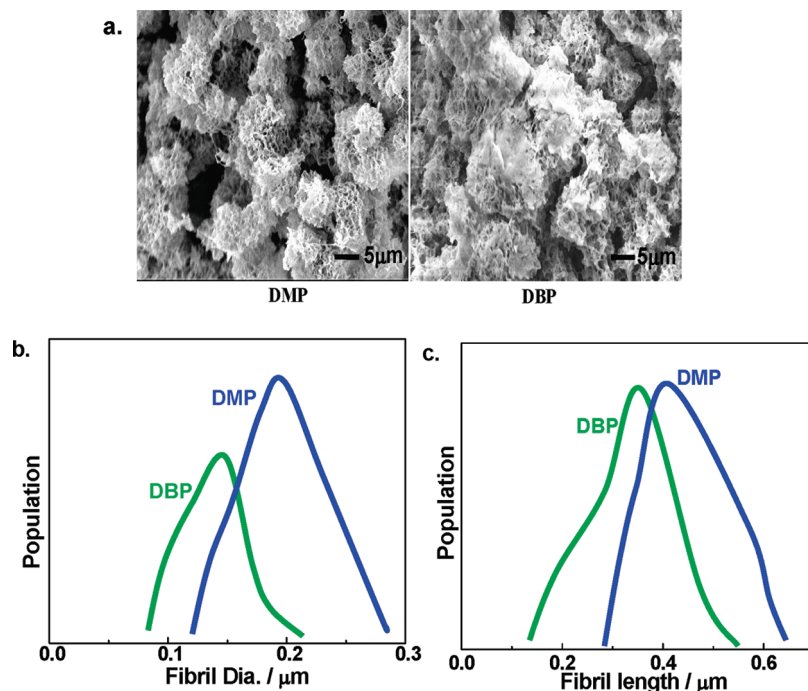


**Figure 3.** (a) SEM micrographs for dried HFP gels in indicated solvents. Distribution of (b) fibril diameter and (c) fibril length obtained in two indicated solvents (polymer concentration was 10% (w/v)).

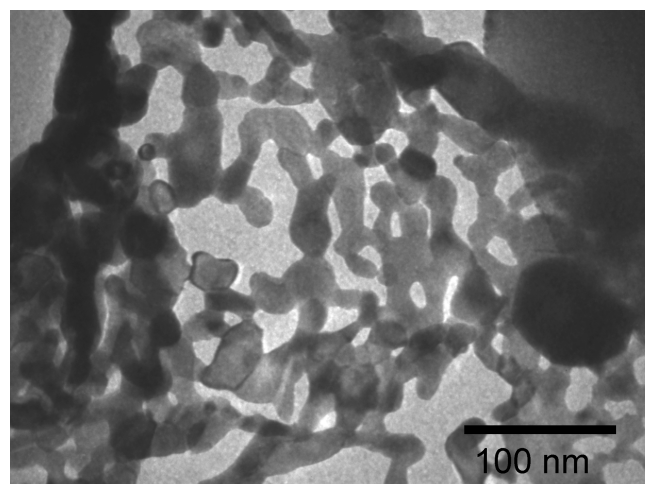


**Figure 4.** TEM bright field image of HFP gel in DMP solvent (dried gel (10% w/v)).

phthalate. It is important to mention that by using low boiling guest solvent (cyclohexane), we are able to keep the original network structure present in gels after removing the guest solvent by evaporation. Direct evaporation of solvent from gels at higher temperature gives the collapsed structure, showing no networking in the dried gel. From the histogram of the fibril diameter and its lateral dimension, the distributions have been shown in Figure 3b. It is evident that the distribution of fibril diameter becomes sharp with increasing “*n*” value of two solvents. Similarly, the lateral dimension of the fibrils has also decreased with increasing “*n*” (Figure 3c). The thicker and wider distribution of fibrils in lower homologues becomes gradually thinner and narrowly disseminated in higher homologues of phthalates. TEM image also supports the fibrillar network formed in dried gel (Figure 4).

**Small-Angle Neutron Scattering.** Fibrillar patterns and their gradual change in dimensions have been shown from morphological studies. So as to look inside the fibrillar morphology, SANS has been measured to inspect the detail structure. Figure

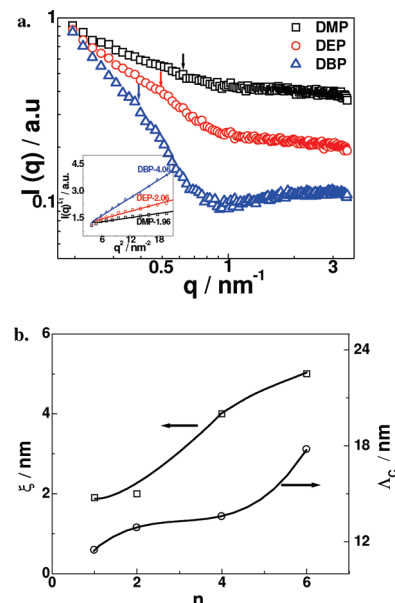


**Figure 5.** (a) Small-angle neutron scattering intensity  $I(q)$  of HFP gels prepared from indicated solvents. The down arrows indicate the peak position. The solid lines in the inset figure represent the Ornstein-Zernike fitting at lower wavevector region. (b) The correlation length and the characteristic length (calculated from the Ornstein-Zernike fitting) as a function of aliphatic chain length of phthalates.

5a shows the small angle neutron scattering patterns of gel prepared from the indicated solvents in the wavevector ( $q$ ) range  $0.17$ – $3.5 \text{ nm}^{-1}$  after the subtraction of background and incoherent scattering from the hydrogen. The error bars of the representative SANS measurement have been shown in Supporting Information Figure S1. Here, it is worthy to mention that the fluorinated copolymer along with its moderately crystalline nature in gels provides better contrast even when the solvents are hydrogeneous. The lower  $q$ -regions (before starting the experimental data points of the shoulder) are best fitted with Ornstein-Zernike model (eq 1), where,  $I(o)$  is the

**TABLE 1: The Correlation Length ( $\xi$ ) and Characteristic Length ( $\Lambda_c$ ) of Gels and Dried Gels in Various Phthalates Obtained from SANS Data**

solvent	$\xi/\text{nm}$		$\Lambda_c/\text{nm}$	
	gel	dried gel	gel	dried gel
DMP ( $n = 1$ )	1.9	14.5	11.5	7.1
DEP ( $n = 2$ )	2.0	16.7	12.9	8.0
DEP ( $n = 4$ )	4.0	21.5	13.6	8.7
DEP ( $n = 6$ )	5.0	24.2	17.8	9.3

extrapolated scattering intensity at zero wavevector and  $\xi$  is the correlation length. Moreover, a shoulder is evident in the middle portion of  $q$  for all solvents.

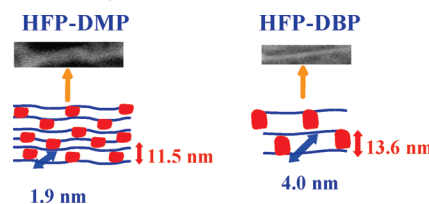
$$I(q) = \frac{I(0)}{1 + \xi^2 q^2} \quad (1)$$

These shoulders are indicative of a stacked lamellar pattern inside the fibril, which is more prominent in Supporting Information Figure S1. Interestingly, the peak position of the shoulders (shown by the arrows) gradually shifted to lower  $q$  range with increasing the aliphatic chain length of diesters. The characteristic lengths,  $\Lambda_c = 2\pi/q_m$ , are 11.5, 12.9, 13.6, and 17.8 nm for DMP, DEP, DBP, and DHP, respectively, where  $q_m$  is the wavevector corresponding to the peak position. The interlamellar distance increases with increasing aliphatic chain length. The correlation lengths,  $\xi$ , have been calculated from lower  $q$ -range by using the Ornstein-Zernike model (inset figure). Nonetheless, significant increase of correlation length is observed 1.9, 2.1, 4.1, and 5.3 nm for DMP, DEP, DBP, and DHP, respectively. The gradual changes of characteristic length ( $\Lambda_c$ ) and correlation length ( $\xi$ ) have been plotted in Figure 5b. As the physical junction points of the HFP gels are crystallites, the correlation length  $\xi$  may be related to the intercrystallite distance.<sup>22</sup> Now, it is obvious that a greater number of physical cross-linking points (lower  $\xi$ ) are formed in case of lower aliphatic chain length containing diester or, in other words, a larger number of junction points are needed to form gel for lower aliphatic chain length diester when compared to solvents with higher " $n$ ". The reciprocal of the square root of the structure factor versus scattering vector has been shown in Supporting Information Figure S2 in order to check the validity of the other models.<sup>29</sup> Very low fitting parameter (0.3–0.5 against the ideal value of 1.0) indicates that the experimental data do not fit the Debye-Bueche model (eq 2) while lower  $q$ -range fits well with Ornstein-Zernike model. The validity of power-law behavior is quite good and the values are nearly constant ~3.8–3.9 (Supporting Information Figure S3).

$$I(q) = \frac{I(0)}{(1 + \xi^2 q^2)^2} \quad (2)$$

The characteristic length,  $\Lambda_c$ , and correlation length,  $\xi$ , for dried gels follow the same trend but different in magnitude and have been presented in Table 1. The difference of gels and dried gels is presumably due to the homogeneous system in gels, as we used the hydrogenated solvent instead of the deuterated one in contrast to a void system in dried gels. The lower values of  $\Lambda_c$  and higher values of  $\xi$  for dried gels in comparison to gels are mainly due to the shrinkage of pattern layers during the removal of solvent molecules and absence of most polymer-solvent complexes to form cross-link points in dried gels,

**SCHEME 2: Comparison of Individual Fibril (Upper Layer, Taken from SEM Micrographs) and Schematic of Lamellar Orientation inside Fibril Showing Self-Assembled Crystallites Size in Indicated Solvents**



respectively. On the basis of the combined SANS results and SEM micrographs, the distribution of lamellae inside each fibril has been shown in Scheme 2 for two phthalates with varying aliphatic chain length " $n$ ". The upper parts of the models are taken from one individual fibril from SEM micrographs of respective solvent. The second layer is the schematic distribution of lamella, which combines together by self-assembling the physical cross-linking points, constructing the above fibril. The black spheres represent the physical junction points and solid lines are the organized lamella. Simultaneously, the interlamellar distance  $\Lambda_c$  and correlation length  $\xi$  increase with increasing aliphatic chain length " $n$ ". It is worthy to mention here that both the characteristic length and correlation length are lower for HFP copolymer as compared to pure PVDF in respective solvent, indicating comparatively poor gel forming capability of HFP than that of pure PVDF.<sup>16</sup> In fact, we observed the same trend in gelation rate in the respective solvent (Supporting Information Figure S4) showing higher gelation rate for pure PVDF in the same concentration and temperature measured. The SANS studies provide the insight lamellar structure of fibril and the correlation length of gels prepared from various phthalates and, thereby, the self-assembled lamellae forming fibrils.

**Small-Angle X-ray Scattering (SAXS).** Figure 6 shows the SAXS scattering profiles of all four dried gels on double logarithmic scale. All the profiles follow straight line, suggesting a power-law behavior ( $I \sim q^{-D}$ ) over a wide  $q$ -range ( $0.03$ – $3.5 \text{ nm}^{-1}$ ). The slope of the lines for all the gels is found to be 3.9, indicating a surface fractal nature with a fractal dimension of 2.12.<sup>30–32</sup> SAXS results on the four samples suggest that the structure of the samples contain regions of high-density polymers, presumably arising from the crystalline fibrils and voids with a rough interface occurs from the interfibrillar region. However, data have not shown any correlation peak within the  $q$ -range of measurement. Nonetheless, the power-law is es-

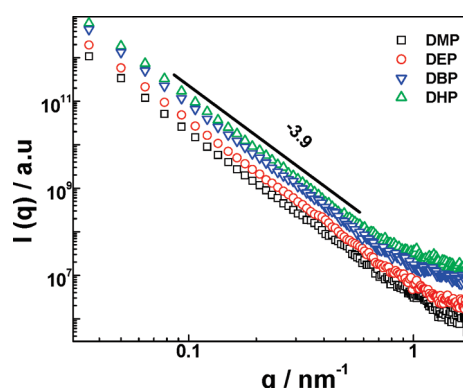


**Figure 6.** Small-angle X-ray scattering intensity  $I(q)$  of HFP dried gels prepared from indicated solvents. The solid lines indicate the slope from the power-law.

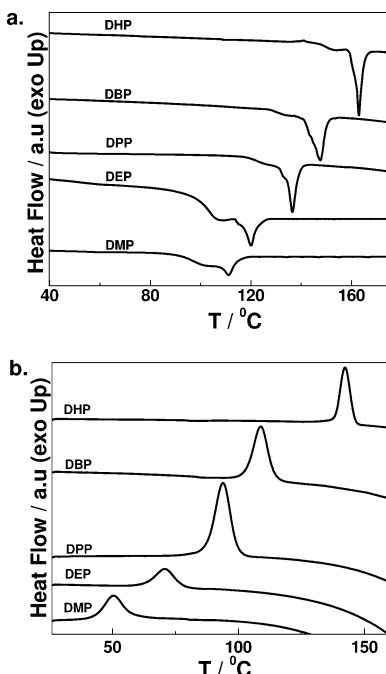


**Figure 7.** DSC thermographs of HFP gels prepared from indicated solvents (a) heating curves and (b) cooling curves. The heating/cooling rate was at 10 °C/min.

sentially the same both for SANS and SAXS studies (supplementary Figure S3).

**Thermal Behavior.** The gel melting behavior in various phthalates has been presented in Figure 7a. The gel melting temperature increases systematically with increasing aliphatic chain length of diester. Usually, HFP shows double melting endotherm, but in gels it might be due to two different kinds of crystallites present in gel phase, apparently exhibited in morphology. The lower endotherm is due to the melting of crystallites embedded in the amorphous zone, giving a weak peak, while the prominent peaks are due to the discrete clusters of crystallites. It is to be noted that low temperature peaks are getting smaller with higher aliphatic chain length, showing more ordered crystallites for higher aliphatic chain length solvent, which is quite obvious from their SEM micrographs. The transformations of sol to gel under controlled cooling have been shown in Figure 7b. Here, the gel formation occurs at higher temperature for higher aliphatic chain length phthalates exhibiting higher gelation rate, which supports the earlier results of gelation kinetics. This behavior indicates the relative rate of gel formation as a function of aliphatic chain length of solvent. The gel melting ( $T_m$ ) and gelation temperature ( $T_{gel}$ ), calculated from the respective peak position, against aliphatic chain length have been plotted in Supporting Information Figure S5, exhibiting increasing tendency of both  $T_m$  and  $T_{gel}$  with " $n$ ". The higher melting temperatures for higher  $n$  suggest that order and thicker crystallites are formed for higher aliphatic chain length phthalates. On the other hand, crystallite formation gets facilitated for higher " $n$ " phthalates. The heat of fusion ( $\Delta H_m$ ) of dried gel and enthalpy of gelation ( $\Delta H_{gel}$ ) has been plotted in Figure 8, revealing increasing tendency with increasing " $n$ ". The gels also show the same tendency of heat of fusion with " $n$ " (inset figure where  $\Delta H_m$  increases with  $n$ ). This clearly suggests that the extent of crystallite formation is more for higher " $n$ " phthalates due to greater interaction between HFP and higher homologues of phthalates as compared to lower " $n$ " phthalates. To understand the interaction between HFP and phthalates and

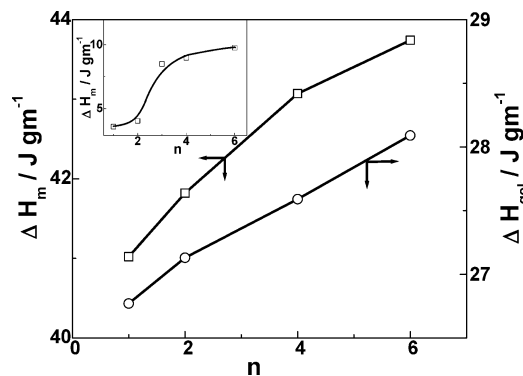


**Figure 8.** The heat of fusion of dried gels ( $\Delta H_m$ ) and the enthalpy of gelation ( $\Delta H_{gel}$ ) for 10% (w/v) HFP as a function of aliphatic chain length of phthalates. The inset figure shows the heat of fusion of gel vs  $n$ .

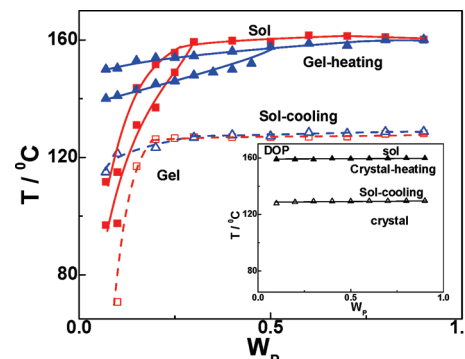


**Figure 9.** Gel melting temperature and gelation temperature vs weight fraction of HFP in gels plot in (solid red square, open red square) DMP, and (solid blue triangle, open blue triangle) DHP. The closed symbols are for gel melting and the open symbols are for gelation temperature. The inset figure is for the crystallization and crystal melting in dioctyl phthalate as gelation phenomena does not occur in DOP.

their compound formations, construction of phase diagrams has been made in different phthalates.

**Thermodynamics and Compound Formation.** Figure 9 shows the phase diagrams of the HFP copolymer gels in DMP and DHP. Both the gel melting temperature ( $T_m$ ) and the gelation temperature ( $T_{gel}$ ) have been plotted with the weight fraction of HFP copolymer ( $w_p$ ). The nature of the curves for  $T_m$  and  $T_{gel}$  is almost same, but there is a difference of  $\sim 30$  °C. It may arise due to the hysteresis effect of the first-order transition and also due to the use of finite rates of heating/cooling. Systems where the phase diagrams obtained on cooling and on heating are very similar and can be regarded as formed under equilibrium.<sup>33,34</sup> Hence, the phase diagrams may be considered to be of the polymer solvent systems formed under equilibrium. The gel melting is lowered with decreasing polymer content. Further, the depression of melting point is more for higher homologue of phthalates due to greater interactions between polymer and solvent at lesser weight fraction of polymer ( $w_p < 0.50$ ). However, the depression is prominent at lower weight fraction of polymer ( $w_p \leq 0.3$ ) for the lower homologue of phthalates as compared to higher  $n$  as the network of the crystallite structure is relatively weak in presence of solvent of lower aliphatic chain length. The same phenomena has been observed in controlled gelation (during cooling) as well. In the case of DOP, which does not form gel, both the temperature curves are parallel to the  $x$ -axis, showing independent melting and crystallization temperature irrespective of the weight fraction of HFP (inset Figure). Here, instead of gel, small crystallites

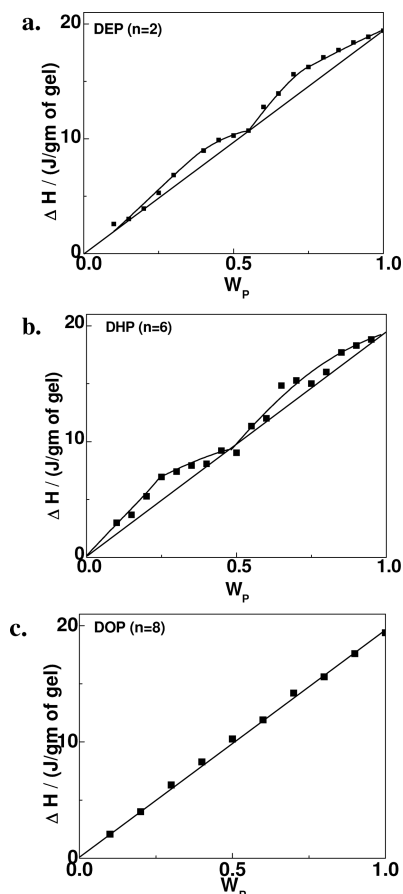


**Figure 10.** The plot of enthalpy changes during the gel melting process of HFP/phthalate gels vs weight fraction of HFP (a) DEP ( $n = 2$ ), (b) DHP ( $n = 6$ ), and (c) DOP ( $n = 8$ ). The solid straight lines indicate the linearity of the enthalpy of solvent and pure HFP. The upper curved lines are guide to eye to observe the change of enthalpy.

are visible even to the naked eye for any concentration of HFP which gives crystallization temperature (lower curve) during cooling and its melting corresponds to the upper curve. There is no depression of melting point and, thereby, exhibiting noninteracting nature between HFP and DOP. On the other hand, both  $T_m$  and  $T_{gel}$  gradually decreases with decreasing HFP content up to 30 wt %, followed by a steep decrease up to 5 wt % or minimum concentration, where gelation can occur, of polymer for all phthalates other than DOP. This decreasing tendency reveal the interacting nature of HFP and phthalates up to  $n = 6$ . The phase diagram of HFP in other phthalates also exhibit similar behavior, and for the sake of clarity we have presented for two phthalates in this case. The phase diagram in DPP has been shown in Supporting Information Figure S6.

The enthalpy of fusion of HFP gels in different phthalates has been plotted in Figure 10 with weight fraction of polymer in gels. In the case of DOP, where gelation does not occur, all the heat of fusion values lie on the line connecting heat of fusion of pure HFP and solvent and  $\Delta H$  follows the linear rule. It has to be mentioned that solvent does not have any heat of fusion in the temperature range studied here. However, other phthalates, where gelation occurs, exhibit a position deviation from the linearity, indicating the formation of compounds of polymer–solvent complexes. We have calculated the heat of fusion of compound formed during gelation by the equation:

$$\Delta H - w_{HFP} \Delta H_{HFP} = \Delta H_{comp} \quad (3)$$

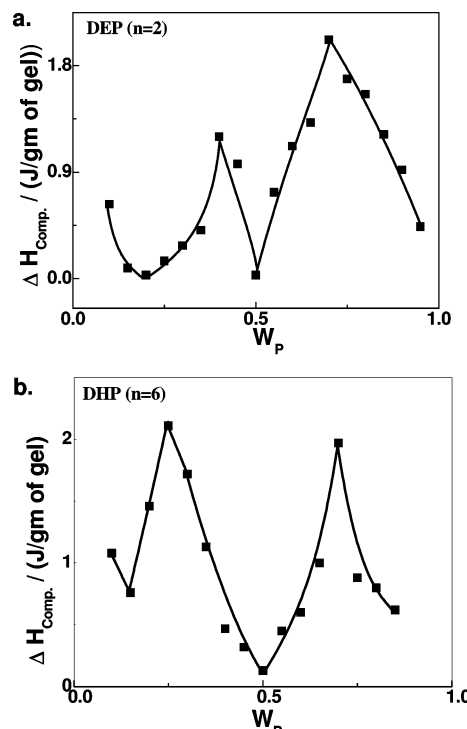


**Figure 11.** Representative plots for the heat of fusion of compounds (polymer–solvent complexes) vs weight fraction of HFP gel (a) DEP ( $n = 2$ ), and (b) DHP ( $n = 6$ ).

Obviously, the measured heat of enthalpy is the summation of the heat of fusion of HFP in that weight fraction plus  $\Delta H$  of compound formed in gels. The positive deviation does show the formation of compound up to DHP ( $n = 6$ ). Interestingly, there are two apparent peaks that might be corresponding to two different compounds in gels, and further, the peaks are becoming prominent with increasing “ $n$ ”, suggesting a greater extent of compound formation for the higher homologue of phthalates. In addition, the deviation of peak position gradually shifts to lower HFP weight fraction with increasing “ $n$ ”. The compositions of the compounds have been measured from the peak of the plot of  $\Delta H_{comp}$  as a function of weight fraction of HFP (Figure 11). There are two prominent peaks suggesting two different compound formations in gel. It is worthy to mention here that prominent double melting endotherms also appear at higher heating rate of 20 °C/min for gels in every solvent. The composition of the compound formed gradually shift to lower weight fraction of HFP with increasing “ $n$ ”. The values are 0.40, 0.35, and 0.25 for DMP, DBP, and DHP, respectively, for lower composition peak and fixed 0.70 for all the phthalates for higher composition peak. The ratios of the monomeric units of HFP and phthalate molecule are 4:1, 5:1, 6:1, and 7:1 for DMP, DEP, DBP, and DHP, respectively, for the higher composition peak ( $w_p = 0.70$ ). In other words, every single phthalate molecule needs 4, 5, 6, and 7 monomeric units to form a complex with DMP, DEP, DBP, and DHP, respectively. The systematic increase of monomeric units per solvent molecule with increasing “ $n$ ” indicates that more number of monomeric units can be surrounded to form the compound for higher homologue of phthalates, suggesting stronger interactions. Similarly, for the lower composition peak ( $w_p = 0.4–0.25$ ), the ratio of the monomeric units of HFP and phthalate molecules is constant at 3:2 for all the phthalates. Dikshit et al.<sup>12</sup> have reported single compound formation (single peak in  $\Delta H_{comp}$  vs  $w_{PVDF}$  curve) for PVDF homopolymer in a series of aliphatic diesters, while the copolymer with HFP in aromatic diesters

exhibits two compounds formation. The compound formation occurs through the complexation of HFP and phthalates, presumably due to the dipole–dipole interaction of  $>\text{C}=\text{O}$  group of phthalates with the  $>\text{CF}_2$  group from the vinylidene fluoride monomeric unit and the  $>\text{C}^*\text{F}_2\text{-CF}(\text{CF}_3)$  group from the hexafluoropropylene monomeric unit of HFP molecules. It is worthy to mention here that pure PVDF forms only one type of compound with phthalates.<sup>35</sup> The reason of forming two different compounds in copolymer lies in the fact that two different type of interactions between  $>\text{CF}_2$  and  $>\text{C}^*\text{F}_2\text{-CF}(\text{CF}_3)$  of two monomers with the  $>\text{C}=\text{O}$  groups of phthalates. The carbon with the star symbol forms another interaction site along with the normal  $>\text{CF}_2$  unit from vinylidene fluoride. The nature of interactions taking place in copolymer and aromatic diester has been discussed in the following section. Aliphatic diester with varying intermittent chain length<sup>12</sup> does not show any systematic shift in compound composition as phthalates, and the reason may lie on the gelation kinetics and dynamics of gelation in two different cases. We have shown that the complex formed from the various trans- forms of phthalates and double-strand  $\alpha$ -PVDP corroborate the experimental observation through semiempirical electronic structure calculation.<sup>16</sup> To have the double-stranded structure, usually the PVDF chains are slightly puckered and oriented in two different directions to accommodate the bulky phthalates, and as a result, the shortest distance between two interactive dipoles is high ( $\sim 3.5 \text{ \AA}$ ) as compared to aliphatic diesters ( $\sim 2.5 \text{ \AA}$ ). Dikshit et al.<sup>12</sup> also showed one by one layered patterns of PVDF chain and aliphatic diester through MMX calculation, which has to be the ideal close-packed structure of PVDF and aliphatic diester solvent. Nonetheless, there is a definite formation of polymer–solvent complex in phthalates, and the compound composition systematically shift to lower molar ratio of monomer per solvent molecules with increasing aliphatic chain length of phthalates. As the interaction for higher homologue of phthalates with HFP is high, a greater number of monomer units can be bounded to form the complex. However, the effect of compound formation on phase diagram and aliphatic chain length of phthalates have been discussed, showing differences in gelation behavior in phthalates with varying “n”. The extent of dipolar interaction between HFP and phthalates increases with increasing “n”, and its quantitative measure might be possible through molecular modeling. However, the two peaks in DSC gel melting can be explained now on the basis of two types of structure formation in HFP–phthalate systems.

**Molecular Modeling.** Designing the model structure of HFP–diester complexes may be obtained by using the semiempirical AM1 (electronic structure calculations) method. Initially, both the structure of polymer and diester was energetically minimized. The diester and HFP molecules can move toward each other either in cis- or trans- conformation as the energy difference between the two is small and conformational transformation may occur during geometry optimization. It is supposed that the interacting sites of HFP and diester are the  $>\text{CF}_2$ ,  $>\text{C}^*\text{F}_2\text{CF}(\text{CF}_3)$  and  $>\text{C}=\text{O}$  moieties, respectively, through which dipole–dipole type of interactions may exist due to electronic polarization. Figure 12 shows the representative optimized complexes in DMP and DHP using the double strand of HFP and phthalates. The dashed lines show the distances between the two nearest interacting sites for two  $>\text{C}=\text{O}$  groups and either  $>\text{CF}_2$  or  $>\text{C}^*\text{F}_2\text{CF}(\text{CF}_3)$  groups of two separate strands of HFP. In one side of diester, the distance with  $\text{CF}_2$  unit of vinylidene fluoride monomer gradually decreases with increasing aliphatic chain length up to  $n = 6$  and then increases with further

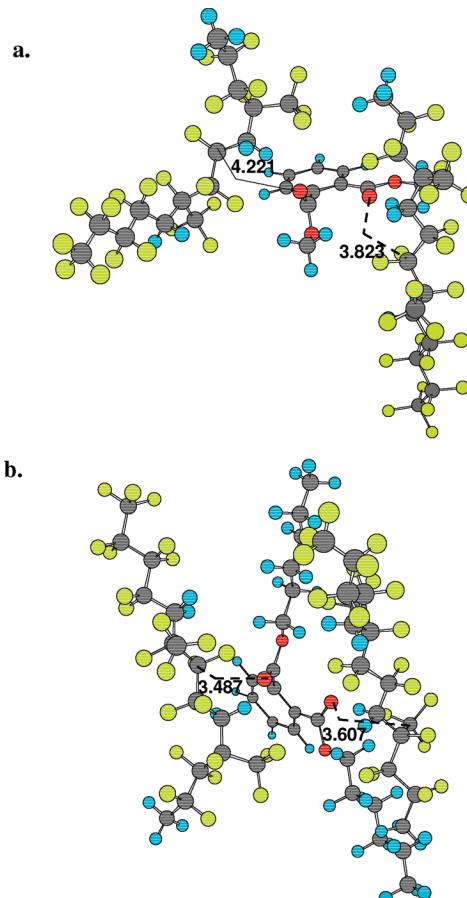


**Figure 12.** Molecular models of HFP–phthalate complexes obtained from energy minimized electronic structure calculation (a) in DMP and (b) in DHP solvent showing the distances between two nearest dipole in both side of the solvent.

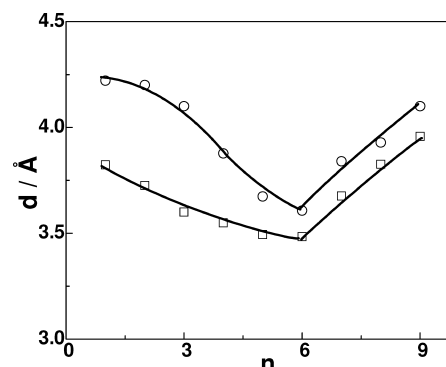


**Figure 13.** Two shorter distances between two interactive dipoles in two different HFP strands in HFP–phthalate complexes in, shown above as a function of aliphatic chain length (n) considering double-stranded models. The solid lines are arbitrarily drawn to show the nature of changes.

increase in  $n$ . On the other side, the distance between  $>\text{C}=\text{O}$  group and either  $>\text{C}^*\text{F}_2\text{CF}(\text{CF}_3)$  of hexafluoropropylene monomer or  $\text{CF}_2$  group of vinylidene fluoride monomer also systematically decreases with increasing  $n$  up to 6, followed by an increasing tendency. The two lower distances of dipoles in two opposite sides of phthalates have been plotted against aliphatic chain length in Figure 13. Interestingly, the distance gradually decreases up to  $n = 6$  and then it starts increasing, presumably due to the lesser interaction in presence of bulkier aliphatic group after the magic number of  $n = 6$ . If we recollect the experimental gelation rate, it increases up to  $n = 6$  and then

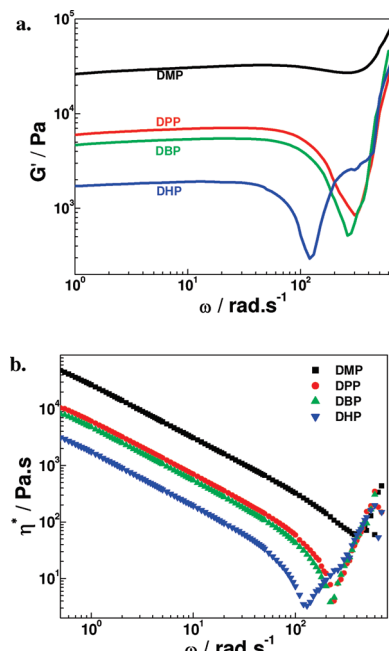


**Figure 14.** (a) Storage modulus ( $G'$ ) and (b) viscosity ( $\eta^*$ ) of HFP gels (10%) prepared from indicated solvents at 40 °C.

it does not form gel at all. The models of the complexes formed from various trans-forms of diesters and double-strand HFP confirm the experimental observation that the gelation rate increases up to  $n = 6$  as the dipolar distances decrease with increasing “ $n$ ”. The two dipoles in opposite sides of the phthalate molecules can explain well the formation of two different compounds, which we got experimentally in thermodynamics of compound formation. As the distances between the  $>\text{CF}_2$ – $>\text{C}^*\text{F}_2\text{CFCF}_3$  of HFP and  $>\text{C=O}$  of diester decrease, stronger complexation may take place up to  $n = 6$  due to the fact that the interaction between HFP and phthalate is dipolar in nature. The complex arising from the interaction of  $>\text{C=O}$  and  $>\text{CF}_2$  unit of vinylidene fluoride constitute the stronger compound as the dipolar distance is minimum in this case and might be the lower polymer composition compound ( $w_p \sim 0.3$ ) due to greater interaction from lower dipolar distance. On the other hand, the complex arising from the interaction of  $>\text{C=O}$  and  $>\text{C}^*\text{F}_2\text{CFCF}_3$  unit hexafluoro propylene comprise the relatively weak compound and might be the higher polymer composition compound ( $w_p \sim 0.7$ ) due to less interaction from the higher dipolar distances. Obviously, the gelation rate will be enhanced gradually for stronger complexes. On the contrary, the dipole distances increase after  $n = 6$ , and as a result, the formation of physical junction points may be hampered, causing no transformation of sol-to-gel. In summary, the molecular modeling suggests that in case of the trans-form, minimum distance of approach of phthalates toward HFP chain initially decreases with chain length of the diester group of phthalate and then increases for  $n > 6$ , passing through a minimum for C<sub>6</sub> carbon chain length that strongly supports the experimental observations. In addition, the modeling and thermodynamics of compound formation corroborate each other and we can assign the composition of the complexes from the dipolar distances in energy minimized state.

**Dynamic Mechanical Properties.** The fibrillar networking and its dimensions in gels with various phthalates may have impact on mechanical properties. The storage modulus,  $G'(\omega)$ , measured at 40 °C, decreases gradually with increasing “ $n$ ” over a wide range of angular frequency  $\omega$  (Figure 14a). The

mechanical properties decreases with increasing aliphatic chain length of phthalates as the fibril dimensions (both diameter and length) have sufficiently been reduced for higher “ $n$ ” (Figure 3b,c). Interestingly, the moduli exhibit a sudden plunge at specific range of  $\omega$  and further increases with increasing frequency. Moreover, the dip has been shifted systematically toward lower frequency for greater “ $n$ ”, indicating the splintering of network depending on the strength of association (superior for lower aliphatic chain length phthalate because of thick fibrillar dimension). The dip in storage modulus in a range of frequency is presumably due to the breakage and subsequently the reformation of structure, suggesting reversible nature of the structure breaking/reformation under frequency sweep. The temperature dependence frequency sweep test indicates that the breakage/alignment of structure occurs easily at higher temperature. Further, the complex viscosity  $\eta^*(\omega)$  shows the similar dip and tendency in viscosity in frequency sweep (Figure 14b) for various gels. The steady shear experiment also exhibits the similar tendency of lowering viscosity with increasing “ $n$ ” (Supporting Information Figure S7). Hence, the mechanical property of gels varies significantly with aliphatic chain length of phthalates depending on the fibrillar dimension and strength.

Hence, the structure, morphology, thermal behavior, dynamic mechanical properties, scattering experiments, and modeling convoluted the gelation behavior, kinetics, and mechanism of HFP gels in various phthalates, and this concept can be extended to other polymer–solvent pairs of similar interacting nature.

## Conclusions

The thermoreversible gelation of poly(vinylidene fluoride-co-hexafluoro propylene) copolymer has been reported in phthalates with varying aliphatic chain length ( $n$ ) of diester. There is a magic number of  $n = 6$  up to which the gelation rate continuously increases with increasing  $n$  while the gelation phenomenon ceases at  $n > 6$ . The fibrillar morphology is apparent in dried gels, and both the thickness and lateral dimension becomes thinner with increasing  $n$ . Small-angle neutron scattering of the gels indicate a sheet-like structure, where the interplaner distance increases with increasing aliphatic chain length of diester. The decrease of scattering intensity  $I(q)$  with the wavevector  $q$  follows the Ornstein–Zernike model, and the correlation length  $\xi$  also increases with increasing “ $n$ ”. SAXS studies support the power-law behavior along with SANS experiment. A schematic has been presented how gels are formed in various phthalates. The melting point and the heat of fusion of gels systematically increase with aliphatic chain length. The phase diagrams of the copolymer gels have been studied in detail, showing two different types of compound formation. A systematic change of compound composition has also been observed for higher composition compound and fixed 3:2 compounds with respect to monomeric unit and solvent molecule was found for lower composition range of all phthalates. On the basis of electronic structure calculations, a model has been proposed to explain the conformation of copolymer chain in presence of various phthalates and finally the polymer–solvent complexes, which further signify the cause of higher gelation rate for higher aliphatic chain length and cessation of gelation process at  $n > 6$ . The formation of two complexes leading to two different compounds with their specific composition has also been verified through thermodynamics and modeling of HFP in phthalates. The mechanical properties vary with the strength of fibrillar pattern exist in gels

and exhibit realignment at particular frequency depending the strength of gels.

**Acknowledgment.** We acknowledge the receipt of research grant from UGC-DAE CSR, Mumbai Centre (project no. CSR/CD/MUM/CRS-M-116). The supply of PVDF samples from Ausimont, Italy, is gratefully acknowledged. We also acknowledge Dr. M. Yashpal and Prof. G. Singh, IMS, BHU, for TEM studies.

**Supporting Information Available:** Detailed description of the figures of SANS studies; behavior of gelation temperature and gel melting as a function of aliphatic chain length; phase diagram and compound formation of HFP in dipropyl phthalate. The shear viscosity of various gels as a function of time. This material is available free of charge via the Internet at <http://pubs.acs.org>.

## References and Notes

- (1) *Thermoreversible Gelation of Polymers and Biopolymers*; Guenet, J. M., Ed.; Academic Press: London, 1997.
- (2) Domzy, R. C.; Alamo, R.; Edwards, C. O.; Mandelkern, L. *Macromolecules* **1986**, *19*, 310.
- (3) *Integration of Fundamental Polymer Science and Technology*; Berghmans, H., Lemstra, P. J., Kleintjens, L. A., Eds.; Elsevier Applied Science: London, 1988, Vol. 2, p 296.
- (4) Paul, D. R. *J. Appl. Polym. Sci.* **1967**, *11*, 439.
- (5) Kawanishi, K.; Komatsu, M.; Inoue, T. *Polymer* **1987**, *28*, 980.
- (6) Komatsu, M.; Inoue, T.; Miyasaka, K. *J. Polym. Sci., Polym. Phys. Ed.* **1986**, *24*, 303.
- (7) *Reversible Polymeric Gels and Related Systems*; Russo, P. S., Ed.; American Chemical Society: Washington, DC, 1987.
- (8) Cho, J. W.; Song, H. Y.; Kim, S. Y. *Polymer* **1993**, *34*, 1024.
- (9) Kim, B. S.; Baek, S. T.; Song, K. W.; Park, I. H.; Lee, J. O.; Nemoto, N. *J. Macromol. Sci., Part B: Phys.* **2004**, *43*, 741.
- (10) Mal, S.; Maiti, P.; Nandi, A. K. *Macromolecules* **1995**, *28*, 2371.
- (11) Mal, S.; Nandi, A. K. *Polymer* **1998**, *39*, 6301.
- (12) Dikshit, A. K.; Nandi, A. K. *Macromolecules* **2000**, *33*, 2616.
- (13) Dasgupta, D.; Nandi, A. K. *Macromolecules* **2005**, *38*, 6504.
- (14) Dasgupta, D.; Manna, S.; Malik, S.; Rochas, C.; Guenet, J. M.; Nandi, A. K. *Macromolecules* **2005**, *38*, 5602.
- (15) Dikshit, A. K.; Nandi, A. K. *Langmuir* **2001**, *17*, 3607.
- (16) Yadav, P. J. P.; Ghosh, G.; Maiti, B.; Aswal, V. K.; Goyal, P. S.; Maiti, P. *J. Phys. Chem. B* **2008**, *112* (15), 4594.
- (17) Saiani, A.; Spevacek, J.; Guenet, J. M. *Macromolecules* **1998**, *31*, 703.
- (18) Malik, S.; Rochas, C.; Guenet, J. M. *Macromolecules* **2005**, *38*, 4888.
- (19) Daniel, C.; Deluca, M. D.; Guenet, J. M.; Brulet, A.; Menelle, A. *Polymer* **1996**, *37*, 1273.
- (20) Daniel, C.; Menelle, A.; Brulet, A.; Guenet, J. M. *Polymer* **1997**, *38*, 4193.
- (21) Poux, S.; Malik, S.; Thierry, A.; Dosiere, M.; Guenet, J. M. *Polymer* **2006**, *47*, 5596.
- (22) Kanaya, T.; Ohkura, M.; Kaji, K.; Furusaka, M.; Misawa, M. *Macromolecules* **1994**, *27*, 5609.
- (23) Abad, L.; Okabe, S.; Koizumi, S.; Shibayama, M. *Physica B* **2006**, *381*, 103.
- (24) Kanaya, T.; Ohkura, M.; Takeshita, H.; Kaji, K.; Furusaka, M.; Yamaoka, H.; Wignall, G. D. *Macromolecules* **1995**, *28*, 3168.
- (25) Motokawa, R.; Annaka, M.; Nakahira, T.; Koizumi, S. *Colloids Surf., B* **2004**, *38*, 213.
- (26) Singh, S. S.; Aswal, V. K.; Bohidar, H. B. *Intl. J. Biol. Macromol.* **2007**, *41*, 301.
- (27) Aswal, V. K.; Goyal, P. S. *Curr. Sci.* **2000**, *79*, 947.
- (28) Schmidt, P. W.; Hight, R., Jr. *Acta Crystallogr.* **1960**, *13*, 480.
- (29) Guenet, J. M. *J. Phys. II* **1994**, *4*, 1077.
- (30) Schmidt, P. W. *J. Appl. Crystallogr.* **1991**, *24*, 414.
- (31) Martin, J. E.; Hurd, A. J. *J. Appl. Crystallogr.* **1987**, *20*, 61.
- (32) Texeira, J. *J. Appl. Crystallogr.* **1988**, *21*, 781.
- (33) Guenet, J. M. *Thermochim. Acta* **1996**, *284*, 67.
- (34) Daniel, C.; Dammer, C.; Guenet, J. M. *Polymer* **1994**, *35*, 4243.
- (35) The  $\Delta H$  vs composition curve for pure PVDF also shows positive deviation with a single compound formation. The peak position of the deviation gradually shifts to lower composition side with increasing aliphatic chain length.

JP907047B